



# Modelling sea-level fingerprints of glaciated regions with low mantle viscosity

Alan Bartholet<sup>1</sup>, Glenn A. Milne<sup>1</sup> and Konstantin Latychev<sup>2</sup>

5 <sup>1</sup> Department of Earth and Environmental Science, University of Ottawa, Ottawa, K1N 6N5, Canada

<sup>2</sup> Department of Earth and Planetary Sciences, Harvard University, Cambridge, MA 02138, USA

*Correspondence to:* Glenn A. Milne (gamilne@uottawa.ca)

**Abstract.** Sea-level fingerprints define the spatially varying relative sea-level response to changes in grounded ice distribution. These fingerprints are a key component in generating regional sea-level projections. Calculation of these fingerprints is commonly based on the assumption that the isostatic response of the Earth is dominantly elastic on century time scales. While this assumption is accurate for regions underlain by mantle material with viscosity close to that of global average estimates, recent work focusing on the Antarctic region has shown that this assumption can lead to significant error when the viscosity departs significantly from typical average values. Here we test this assumption for fingerprints associated with glaciers and ice caps. We compare output from a (1D) elastic Earth model to that of a 3D viscoelastic model which includes low viscosity mantle in three glaciated regions: Alaska, southwestern Canada and the southern Andes (Randolph Glacier Inventory (RGI) regions 1, 2 & 17, respectively). This comparison indicates that the error incurred by ignoring the non-elastic response is generally less than 1 cm over the 21st century but can reach magnitudes of up to several 10s of centimetres in low viscosity areas. This error can have large spatial gradients where crustal uplift in ice covered (or previously ice covered) areas changes into subsidence when moving away from the loading centres to areas peripheral to the mass loss. The existence of these large gradients indicates the need for loading models with high spatial resolution to accurately simulate sea-level fingerprints in these regions. We conclude that sea-level projections for Alaska, southwestern Canada and the southern Andes should not be based on elastic Earth models.

## 1 Introduction

A variety of processes drive changes in the height of the ocean floor and ocean surface (e.g. Church et al., 2013; Milne et al., 2009), and the combination of these processes produces a complex pattern of sea level change that varies through time as the relative contribution of each process often changes. While the global average relative sea-level change provides a useful single value which reflects the contribution from climate-related processes, specifically land ice melt and ocean warming, and does represent a good estimate of sea level change at many coastal locations, various regional processes that produce a strong signal can result in large departures from the global average value (Church et al., 2013). As a result, predicting future sea-level changes at regional to local scales is challenging as it requires calculating the signal associated with numerous physical



processes that have a range of spatial scales and response times and then summing the results (Slangen et al., 2011; 2014; Kopp et al., 2014).

35 Around the world, glaciers and ice sheets are losing mass and retreating (e.g. Oppenheimer et al., 2019; Vaughan et al., 2013; Shepherd et al., 2018; 2020; Wouters et al., 2019; Zemp et al., 2019). Observations since 1850 show that, on a global scale, the rate of glacier mass loss in the early 21st-century is without precedent for the observation period (and potentially for all recorded history) (Zemp et al., 2015). The melting of ice sheets and glaciers produces a complex pattern of sea level change due to the resulting solid Earth deformation and changes to the geopotential (Farrell and Clark, 1976). When these changes happen on decadal to centennial time scales the resulting solid Earth response is dominantly elastic and so the non-elastic (viscous) component is commonly ignored. The modelled spatial patterns in relative sea-level change associated with these short-term changes in ice mass are often termed "sea-level fingerprints" (e.g. Mitrovica et al., 2011). These fingerprints play a central role in projections of regional sea-level change (Church et al., 2013; Oppenheimer et al., 2019; Slangen et al., 2012; 2014; Spada, 2017).

45 The assumption of an insignificant contribution of the non-elastic signal to sea-level fingerprints was recently addressed in a paper focusing on mass loss of the Antarctic ice sheet (Hay et al., 2017). The viscosity of the Earth's mantle is known to be several orders of magnitude lower than that of the global average in this region (e.g. Whitehouse et al., 2019). Hay et al. (2017) concluded that the viscous component of the response is significant and so should be included when computing sea-level fingerprints. In this study, we address the same question but focus on regions with glaciers that are underlain by low viscosity mantle rock. Recent studies have provided evidence that the glaciated regions of Alaska, Western Canada & USA and the Southern Andes are located in regions where the sub-lithosphere mantle viscosity is several orders of magnitude lower than typical global mean values (e.g. Hu and Freymuller, 2019; James et al., 2009; Jin et al., 2017; Richter et al., 2016). The cause of such low viscosity is believed to be related to the presence of plate subduction in these areas. Departure from an elastic response will be relatively large in these regions and so the computed sea-level fingerprints may be in significant error. The primary aim of this work is to quantify the amplitude and spatial extent of the error caused by assuming an elastic Earth response in the three regions mentioned above. In particular, a key goal is to determine if the influence of these low viscosity regions extends significantly beyond the regions defined by low viscosity mantle material.

## 2 Methods

Our sea-level projections were generated using a numerical finite-volume formulation of the surface loading process (e.g. Latychev et al., 2005; Hay et al., 2017). This formulation assumes a spherical Maxwell body, filled by tetrahedral elements in which the lateral resolution is greatest (~12 km) near the surface of the Earth model and lowest (~50 km) at the core-mantle boundary. Immediately beneath the surface, the depth resolution is ~12 km, compared to ~50 km immediately above the core-



mantle boundary. The sea-level algorithm used in our GIA model is based on the theory described in Mitrovica and Milne (2003) and described in Kendall et al. (2005) but extended to incorporate the influence of Earth rotation on RSL changes (Milne and Mitrovica, 1998; Mitrovica et al., 2005). In order to apply this algorithm, two primary inputs must be defined: a realistic space-time evolution of grounded land ice to force the model and a realistic model of the Earth that defines the interior density and rheology structure to compute the isostatic response. These two model inputs are detailed below.

## 2.1 Ice model

In this study we created ice models for each of the 19 first order regions in the Randolph Glacier Inventory 5.0 (RGI; Pfeffer et al., 2014). The RGI provides the area of glacier extent in each of the regions and then we apply the region-specific thickness-area scaling function of Huss and Farinotti (2012) which calculates the mean thickness of each glacier in a region using:

$$\bar{h} = cS^\gamma \quad (1)$$

where  $\bar{h}$  is the mean thickness,  $S$  is the area of the glacier, and  $c$  and  $\gamma$  are constants specific to each region in the RGI. In order to determine a mass loss history for our ice model for all 19 regions in the RGI we use the decadal Representative Concentration Pathway (RCP) 4.5 projections provided by Huss and Hock (2015) for the period 2010-2100 CE with a net global barystatic (Gregory et al., 2019) sea-level change of 10.8 cm.

Using the decadal mass loss projections we produced a model of ice extent changes that simulates the vertical thinning of the GICs as well as a crude estimate of lateral retreat as the area of ice cover changes. We iterated over each of the decadal time steps and calculated the amount of uniform ice thickness change (based on areal extent) required to equal the projected sea-level equivalent (SLE) using a tolerance of  $\pm 1$  %. We then subtracted this height from the ice thickness distribution of the previous time step and revised the area distribution to account for locations where ice thickness had reduced to zero. We then applied a spatial Gaussian filter to the calculated change in ice extent between successive time steps (using NumPy 1.16.1 Multidimensional Gaussian filter) to spatially smooth the ice thickness distribution. While this did result in some loss of spatial fidelity, it removed large spatial gradients in the ice thickness distribution that were unphysical. This process was applied individually to each of the 19 first order regions in the RGI. Figure 1a shows ice extent at 2010 and 2100 CE for the RGI regions 1 (Alaska) & 2 (Western Canada and USA) and Figure 1b gives the same results for region 17 (Southern Andes).

## 2.2 Earth model

The density and elastic properties of our Earth model are defined using the radial (1D) seismic Preliminary Reference Earth Model (Dziewonski and Anderson, 1981). We note that the influence of lateral variations in elastic and density structure on the computation of sea-level fingerprints has been shown to be negligible (Mitrovica et al., 2011). Due to large uncertainty in our knowledge of the viscosity structure of the Earth, the viscosity structure is most commonly defined by only three parameters: the first is an outer shell of high viscosity ( $1 \times 10^{37}$  Pa s) which is used to simulate an elastic outer shell (the



lithosphere); the second is an isoviscous upper mantle region which extends from the base of the lithosphere to a depth of 670  
95 km; and third, an isoviscous lower mantle region that extends from 670 km to the core-mantle boundary (2885 km). The  
values used to define the viscosity vary depending on the region detailed below resulting in an Earth model where the internal  
viscosity structure varies not only with depth but laterally as well. In contrast, the surface features of the Earth model (e.g., ice  
extent, topography) vary as a function of time and geographic position.

100 In defining global-scale viscosity structure, we assign a lithospheric thickness of 96 km, an upper-mantle viscosity of  $5 \times 10^{20}$   
Pa s, and a lower-mantle viscosity of  $1 \times 10^{22}$  Pa s. While there is considerable uncertainty in our knowledge of global average  
viscosity structure, the majority of this uncertainty relates to that of the lower mantle (e.g. Mitrovica and Forte, 2004; Lambeck  
et al., 2014). The values we use for lithospheric thickness and upper mantle viscosity are broadly compatible with those from  
recent analyses of global GIA data sets (Lambeck et al., 2014; Peltier, 2004) and the value we use for lower mantle viscosity  
105 represents a middle ground between these recent estimates. Given short time period of our model simulation (~100 yr), the use  
of other global average viscosity structures could be substituted without significantly impacting the results as the component  
of non-elastic deformation is small for viscosity values typically inferred in global GIA analyses. The regional viscosity  
structure we adopt is the more important aspect of our Earth model as this is anomalously low in RGI regions 1, 2 & 17.

110 For RGI region 1 (Alaska), a number of studies have estimated the regional viscosity structure (e.g. Larsen et al., 2005; Sato  
et al., 2011; Jin et al., 2017; Hu and Freymueller, 2019). All of these studies estimate a relatively thin lithosphere elastic  
thickness, averaging around 50 km but with uncertainty of a few 10s of km, and low viscosity values in the shallow upper  
mantle ranging between middle  $10^{18}$  Pa s to low  $10^{19}$  Pa s. In a relatively recent analysis, Jin et al. (2017) used measurements  
from Ice Cloud and Land Elevation Satellite (ICESat), global positioning system (GPS), and Gravity Recovery and Climate  
115 Experiment (GRACE) to estimate a number of ice and Earth model parameters. By isolating the signal due to past ice loading,  
they concluded on a best fit three-layer Earth model consisting of a lithospheric (elastic) thickness of 60 km, a 110 km thick  
asthenosphere with a viscosity of  $2 \times 10^{19}$  Pa s, and a sub-asthenosphere mantle with a viscosity of  $4 \times 10^{20}$  Pa s. A more recent  
study (Hu and Freymueller, 2019) also used vertical land motion rates from GPS to constrain regional, depth-dependent  
viscosity structure. They estimated lithosphere thickness to be 55 km and the viscosity and thickness of the asthenosphere to  
120 be, respectively,  $3 \times 10^{19}$  Pa s and 230 km, but noted a significant trade-off in these parameter values.

While there is a considerable degree of uncertainty in defining model parameters for this region, the relatively good agreement  
between these two recent studies gives some confidence in choosing parameters. We adopted the values of Jin et al. (2017) for  
this study (those from Hu and Freymueller (2019) were published after the completion of our modelling) and extended their  
125 sub-asthenosphere region (with a viscosity of  $4 \times 10^{20}$  Pa s) to the bottom of the upper mantle (670 km); below this depth  
values associated with the global background model are the default. The lateral extent of these viscosity values at the model  
Earth surface is shown in red in Figure 2a. In order to constrain the lateral extent of the low viscosity region we define a surface



area that is roughly similar to the region studied by Jin et al. (2017). Note that the extent of this region decreases with depth to ensure that the proportion of this region relative to the global area at a given depth remains constant.

130

For RGI region 2 (Western Canada & USA), we are interested only in the area adjacent to southwestern British Columbia as this is where GIA studies have inferred low viscosity values: James et al. (2009) concluded that RSL observations from Vancouver Island can be fit equally well across a wide range of asthenosphere thicknesses and viscosities. The Earth model with the lowest viscosity consisted of a lithospheric (elastic) thickness of 60 km, a 140 km thick asthenosphere with a viscosity of  $3 \times 10^{18}$  Pa s, and a sub-asthenosphere mantle with a viscosity of  $4 \times 10^{20}$  Pa s. These results are supported by a more recent study that considered sea-level observations from a larger area in southwestern British Columbia (Yousefi et al., 2018) and so we adopt the values from James et al. (2009) to define the regional lithosphere thickness and upper mantle structure. The lateral extent of this region at the model Earth surface is shown in green in Figure 2a.

135

140

In the southern Andes region (RGI area 17), a number of studies have inferred the presence of low viscosity mantle rock (e.g. Ivins and James, 1999; Ivins and James, 2004; Lange et al., 2014; Richter et al., 2016) that likely resides in the mantle wedge between the subducting plate and the base of the lithosphere (Klemann et al., 2007). In all of these studies, the estimated lithosphere elastic thickness is relatively thin (~30 km) and asthenosphere viscosity low (order  $10^{18}$  Pa s). We adopted results from the most recent of the above-listed analyses, Richter et al. (2016), who used observations from 43 geodetic Global Navigation Satellite System (GNSS) sites distributed over the Southern Patagonian Ice Field to analyze vertical and horizontal velocities of present-day crustal deformation. By applying an ice-load history that assumes a moderate present-day glacial mass loss, with slightly higher than present-day mass loss immediately following the Little Ice Age (LIA) maximum, Richter et al. concluded on a preferred Earth model consisting of a 36.5 km thick lithosphere and a sub-lithosphere mantle with a viscosity of  $1.6 \times 10^{18}$  Pa s. The lateral extent of these viscosity values at the model Earth surface is shown in red in Figure

145

150

### 3 Results and Discussion

Our goal is to quantify the signal of the non-elastic response to sea-level fingerprints computed for the three RGI regions introduced above. Therefore, in the following, we compare results from our 3-D viscoelastic Earth model to those computed assuming the Earth response to the loading changes is elastic.

155

Figure 3a shows the global sea-level fingerprint for the non-linear mass loss results of Huss and Hock (2012) as applied to all regions of the RGI assuming Earth deformation is entirely elastic. As is conventional, the fingerprint shows the total sea level change between the start and end of the study period (in this case, 2010 to 2020 CE). The pattern of sea-level change is typical in that it shows a sea level fall near the sources of the ice mass loss and a sea level rise in the far-field (e.g. Mitrovica et al.,



160 2001). Using the same ice loading model, results for the 3D viscoelastic Earth model are shown in Fig. 3b. At the global scale, comparison between the results in Figs 3a & 3b shows that the differences are small; therefore, we subtract the elastic results from the viscoelastic results (Fig. 3c) to isolate the difference. In Figure 3c, at locations on the order of 1000 km or more away from the ice load, the difference between the viscoelastic and elastic Earth models is negligible (less than 1 cm at 2100 CE). At locations peripheral to glaciated region, the difference is generally within a few cm, with the largest differences evident in  
165 the areas underlain by low viscosity mantle material. In glaciated regions where the viscosity structure is that of the global model (i.e. all RGI regions except 1, 2 & 17), there is a difference of 1-2 cm between the elastic and viscoelastic results indicating that the assumption of an elastic Earth is relatively accurate even in near-field regions when the viscosity of underlying mantle is close to global average values. However, at locations inside the boundaries depicted in Figure 2 (the “near-field”), the difference in sea-level change can be several times larger than the barystatic value (10.8 cm) due to the faster  
170 response times of the low viscosity mantle. Thus, the error introduced by considering only the elastic solid Earth response is spatially restricted and reaches the several cm level only in the vicinity of the low viscosity regions. The remainder of this section will focus on the signal in these near-field regions only.

Sea-level predictions for the elastic and viscoelastic Earth models, as well as the difference between them, for the regions with  
175 underlying low viscosity mantle are shown in Figure 4. A map showing the results for Alaska and Western Canada & USA (Figure 4a-c), indicates that the spatial pattern associated with the viscoelastic signal is markedly different than that for the elastic Earth model. Note that, for ease of interpretation, the predictions shown in Figure 4 consider only the RSL change associated with ice mass loss in the respective RGI regions (1, 2 in Fig. 4a-c and 17 in Fig. 4d-f), hence the difference between the results in Figs 3 & 4. The influence of ice changes in other RGI regions will cause an almost uniform signal over each of  
180 the areas shown in Fig. 4, with amplitude close to the global barystatic value, and so the spatial patterns (gradients) will not be significantly affected by this omission.

Inspection of Fig. 4 indicates that the spatial pattern associated with the viscoelastic signal is markedly different to that of the elastic Earth model. In particular, when an elastic model is used, the near-field RSL signal is entirely negative reflecting  
185 subsidence of the geoid (dominated by ice mass loss) and uplift of the solid Earth. In the viscoelastic case, when there is sufficient time for the non-elastic component of deformation to become significant, a zone of solid Earth subsidence peripheral to the ice covered region becomes apparent, particularly in RGI region 1. These so-called ‘peripheral bulges’ are a characteristic feature of the GIA response on millennial time scales (e.g. Peltier, 1974; Clark et al., 1978; Whitehouse et al., 2018) and reflect the isostatic signal of a thin elastic lithosphere overlying a viscoelastic mantle within which the non-elastic  
190 component of deformation is significant (i.e. close to or exceeding the Maxwell time of the deforming material).

Focusing first on the results for RGI regions 1 & 2 (Fig. 4a-c), in areas where ice has thinned or disappeared (Fig. 1), the RSL change is less than that of the elastic case whereas peripheral to this area, the RSL change is greater. This pattern is somewhat



intuitive when one considers the peripheral bulge effect noted above and the faster response time of the low viscosity material.  
195 Because of the considerably lower mantle viscosity in these regions, the solid Earth responds faster than it otherwise would  
have over the same time period. As a result, the areas shaded in red show a greater sea level fall compared to the elastic case  
due to the additional uplift of the solid Earth surface associated with non-elastic deformation. The peripheral areas showing an  
enhanced sea-level rise (blue colour in Fig. 4a) relate to deformation associated with the peripheral bulge. In these peripheral  
areas, solid surface uplift occurs during loading followed by subsidence once unloading becomes dominant. Thus, the predicted  
200 sea-level fall is related to subsidence of the peripheral bulge that is active following the onset of sustained ice mass loss. The  
error made by assuming an elastic Earth response can exceed several 10s of cm and be positive or negative depending on  
location relative to the transition from uplift to subsidence (red to blue colour in Fig. 4). Of note are the large gradients in the  
RSL response when transitioning between uplifting and subsiding regions.

205 The above interpretation assumes that the differences in RSL are dominated by changes in vertical land motion rather than in  
sea-surface height (due to gravitational changes associated with the Earth deformation). Model output of vertical land motion  
and sea-surface height change, support this interpretation and show that the sea surface component is, in general, smaller than  
the land motion signal but this is site and time dependent (see Fig. 5 and related discussion below).

210 Results for the Southern Andes (Figure 4d-f) are similar in that the non-elastic component of deformation in this region results  
in a more rapid sea-level fall in areas of ice thinning/retreat. The RSL differences (compared to the elastic case) are not as  
large as for RGI region 1 as the amplitude of mass loss is less (Fig. 1), but the differences still reach values of up to 10s of cm  
and so are large. The influence of the peripheral bulge is more subtle than for RGI region 1. This is due to the different  
amplitude and geometry of ice mass loss (Fig. 1) and the difference in the viscosity structure of the asthenosphere and upper  
215 mantle in the regional Earth models. In the model for Alaska, the viscosity model includes a relatively thin (110 km) low  
viscosity asthenosphere overlying an upper mantle with viscosity close to that of the global average. In comparison, the  
regional model for the Southern Andes do not differentiate between the asthenosphere and upper mantle and so a low viscosity  
is defined from the base of the lithosphere to the bottom of the upper mantle. The more restricted depth extent of the low  
viscosity region for Alaska would lead to a stronger component of lateral (channel) flow which would affect the amplitude and  
220 spatial extent of the peripheral bulge.

The spatial patterns shown in Fig. 4 are complemented by model output of time series for six different towns or cities  
(population ranging from ~10,000 to several million inhabitants) in Fig. 5. These particular locations were chosen to illustrate  
the range of RSL signals evident in these near-field areas. RSL time series for RGI regions 1 & 2 are shown for Juneau and  
225 Sitka (Region 1), Vancouver and Victoria (Region 2), and Puerto Natales and Río Grande (Region 17). Time series for both  
the elastic and viscoelastic cases are based on a 10-year discretization of the ice thickness model as described in Section 2.1.  
At Juneau, USA, a sea-level fall is predicted for both the elastic (solid green line) and viscoelastic (solid red line) with the



latter showing a significantly greater fall (by  $\sim 74$  cm). The dashed and dash-dotted red lines show the component signals for the viscoelastic case and these indicate that the vertical land motion (VLM) component dominates over SSH change at this site. Thus, the application of an elastic Earth model greatly underpredicts the sea-level fall at this location. The predicted RSL curves for Puerto Natales are similar in that a sea-level fall is also shown; the amplitude is significantly smaller, however, reflecting the smaller ice mass change in this region and the location of the settlement relative to the area of mass loss, with the viscoelastic case exceeding the elastic by only 4-5 cm.

At Sitka, Vancouver, Victoria and Río Grande, results for the viscoelastic Earth model give an RSL response that transitions from a fall to a rise. This is due to the more complex spatial pattern of the predicted response when a viscoelastic Earth model is applied that has an overlying elastic lithosphere. As noted above, the GIA response is characterised by regions of uplift and subsidence and the so-called “hinge line” that separates these regions. Over the modelled period, the hinge line will migrate towards the main centre of loading over time as the ice retreats and the area of ice cover diminishes. All of these sites are located near the hinge line and so the RSL response transitions from a fall (uplift) to a rise (subsidence) during the 21<sup>st</sup> century. Looking at the results for these four locations, the non-monotonic nature of the RSL response is governed by that of the VLM; the SSH contribution is primarily that of a sea-level fall associated with the reduction in ice mass resulting in a diminishing gravitational pull on the surrounding ocean. This fall in SSH offsets some of the sea-level rise caused by the VLM in these locations. The non-monotonic shape of the RSL curve has the net effect of resulting in a relatively small RSL change over the 21<sup>st</sup> century – at all four sites, the amplitude of RSL change is no more than a few cm. As a consequence, the final difference between the elastic and viscoelastic curves at 2100 CE is also relatively small, except in Sitka where the a RSL rise of  $\sim 4$  cm for the viscoelastic model compares to a large fall of  $\sim 22$  cm for the elastic case.

The results shown in Figs 4 & 5 demonstrate that non-elastic deformation can lead to a near-field RSL signal of up to 10s of cm depending on the site location and the magnitude and distribution of regional ice mass loss. In all cases, the elastic model predicts a RSL fall due to the regional ice mass loss, whereas a sea-level rise can result in some localities when the non-elastic signal is considered (e.g. Sitka, Victoria). The large spatial gradients in the predicted viscoelastic RSL response reflects the short wavelengths in the surface load and the thin lithosphere in these tectonically active regions. Given this, the application of a global-scale model, with limited spatial resolution, is not an optimal approach to determine accurate predictions of future RSL change in these near-field regions. As a result of the limited spatial resolution of our model, Iceland, which is known to be underlain by low viscosity mantle, was not included in the analysis. Further work should focus on the use of global models with non-uniform grids (e.g. Larour et al, 2017) or nested, high-resolution regional grids (e.g. Goldburgh et al., 2016) to more precisely define the radial and lateral boundaries of the low viscosity regions as well as the ice extent model. Additionally, in regions where subduction is occurring it may be beneficial to explicitly incorporate the geometry of the subducting plate into the model (e.g. Austermaann et al., 2013), rather than the simpler 1-D profiles adopted here.



The large amplitude of the non-elastic signal on century time scales in low viscosity regions indicates that application of an elastic model can result in significant error in the calculated sea-level fingerprint. A second important implication of this result is that the isostatic response to the large mass loss changes of the 20<sup>th</sup> century will be considerable and perhaps a dominant contributor to the RSL response during the 21<sup>st</sup> century. The importance of this earlier loading signal is evident in the large contemporary uplift rates measured in the regions considered (e.g. Huy and Freymueller, 2019; Richter et al., 2016). We note that this signal is generally not captured accurately in the global scale GIA models most commonly used in generating regional sea-level projections (e.g. Slangen et al., 2014).

While this study assumes a Maxwell rheology, it is possible that, on the relatively short time scales considered here, significant departures from this relatively simple rheological model may occur. These departures could take the form of a transient component of the non-elastic response (e.g. Yuen et al., 1986; Pollitz, 2005), in which the viscosity increases with time or a power-law response that is often associated with relatively large deviatoric stress (e.g. Wu and Wang, 2008; Van de Wal et al., 2013) for which the effective viscosity would increase as stress levels relax. The significance of these more complex rheological models in low viscosity regions would be a natural extension of this analysis.

#### 4 Conclusions

Sea-level fingerprints are an integral aspect of calculating regional variations in future sea-level change. Calculation of these fingerprints commonly assumes that the isostatic response of the Earth is elastic on century time scales. Here we tested this assumption by comparing output from a (1D) elastic Earth model to that of a 3D viscosity elastic model which includes low viscosity mantle in three glaciated regions: Alaska, southwestern Canada and the southern Andes (RGI regions 1, 2 & 17, respectively). This comparison indicates that the error incurred by ignoring the non-elastic response is generally less than 1 cm over the 21<sup>st</sup> century (but can exceed this in some RGI regions) but can reach magnitudes of up to several 10s of centimetres when proximal (less than ~1000 km) to the three low viscosity areas. This error can have large spatial gradients where crustal uplift in ice covered (or previously ice covered) areas changes into subsidence when moving away from the loading centres to areas peripheral to the mass loss. The existence of these large gradients indicates the need for loading models with high spatial resolution to accurately simulate sea-level fingerprints in these regions. We conclude that sea-level projections for Alaska, southwestern Canada and the southern Andes should not be based on elastic Earth models. Also, the low mantle viscosity in these regions will result in glacier changes during the 20<sup>th</sup> century dominating the GIA signal and so it is critical that the recent mass loading history (past few centuries) is captured in GIA models applied to estimate future sea-level change in these areas. The impact of low Earth viscosity in these three regions has clear implications for the estimation of sea-level hazard and thus policy decisions on coastal management procedures.



## References

- Austermann, J., Mitrovica, J.X., Latychev, K., and Milne, G.A.: Barbados-based estimate of ice volume at Last Glacial Maximum affected by subducted plate, *Nat. Geosci.*, 6, 553, 2013.
- 295 Church, J.A., Clark, P.U., Cazenave, A., Gregory, J.M., Jevrejeva, S., Levermann, A., Merrifield, M.A., Milne, G.A., Nerem, R. S., Nunn, P.D., Payne, A.J. Pfeffer, W.T., Stammer, D., Unnikrishnan, A.S.: Sea Level Change. In *Climate Change 2013: The Physical Science Basis. Contribution of Working Group I to the Fifth Assessment Report of the Intergovernmental Panel on Climate Change*, edited by T.F. Stocker, D. Qin, G.-K. Plattner, M. Tignor, S.K. Allen, J. Boschung, A. Nauels, Y. Xia, V. Bex, and P.M. Midgley, 1137–1216. Cambridge, United Kingdom; New York, NY, USA: Cambridge University Press, 2013.
- 300 Clark, J.A., Farrell, W.E., and Peltier, W.R.: 1978. Global changes in postglacial sea level: a numerical calculation, *Quat. Res.*, 9, 265–287, 1978.
- Dziewonski, A.M. and Anderson, D.L.: Preliminary reference Earth model, *Phys. Earth Planet. Int.*, 25, 297–356, 1981.
- Farrell, W.E. and Clark, J.A.: On Postglacial Sea Level, *Geophys. J. Int.* 46, 647–667, 1976.
- 305 Goldberg, S.L., Lau, H.C.P., Mitrovica, J.X., and Latychev, K.: The timing of the Black Sea flood event: Insights from modeling of glacial isostatic adjustment, *Earth Planet. Sci. Lett.*, 452, 178–184, 2016.
- Gregory, J.M., Griffies, S.M., Hughes, C.W., Lowe, J.A., Church, J.A., Fukimori, I., Gomez, N., Kopp, R.E., Landerer, F., Le Cozannet, G., Ponte, R.M., Stammer, D., Tamiseia, M.E., van de Wal, R.S.W.: Concepts and Terminology for Sea Level: Mean, Variability and Change, Both Local and Global, *Surv. Geophys.*, 40, 1251–1289, 2019.
- 310 Griggs, G.: *Coasts in Crisis: A Global Challenge*, Univ of California Press, 2017.
- Hay, C., Lau, H.C.P., Gomez, N., Austermann, J., Powell, E., Mitrovica, J.X., Latychev, K., and Wiens, D.A.: Sea level fingerprints in a region of complex Earth structure: The case of WAIS, *J. Climate*, 30, 1881–1892, 2017.
- Hu, Y., and Freymueller, J. T.: Geodetic observations of time-variable glacial isostatic adjustment in Southeast Alaska and its implications for Earth rheology. *J. Geophys. Res. – Solid*, 124, 9870–9889, <https://doi.org/10.1029/2018JB017028>, 2019.
- 315 Huss, M. and Farinotti, D.: Distributed ice thickness and volume of all glaciers around the globe, *J. Geophys. Res. – Earth*, 117, F04010, doi:10.1029/2012JF002523, 2012.
- Huss, M. and Hock, R.: A new model for global glacier change and sea-level rise, *Front. Earth Sci.*, 3:54.doi: 10.3389/feart.2015.00054, 2015.
- Ivins, E., James, T.: Simple models for late Holocene and present-day Patagonian glacier fluctuations and predictions of a geodetically detectable isostatic response. *Geophys. J. Int.*, 138, 601–624, 1999.
- 320 Ivins, E., James, T.: Bedrock response to Llanquihue Holocene and present-day glaciation in southernmost South America. *Geophys. Res. Lett.*, 31, L24613, <http://dx.doi.org/10.1029/2004GL021500>, 2004.



- James, T.S., Gowan, E.J., Wada, I., and Wang, K.: Viscosity of the Asthenosphere from Glacial Isostatic Adjustment and Subduction Dynamics at the Northern Cascadia Subduction Zone, British Columbia, Canada, *J. Geophys. Res. – Solid*, 114, B04405, doi:10.1029/2008JB006077, 2009.
- 325 Jin, S., Zhang, T.Y., and Zou, F.: Glacial Density and GIA in Alaska Estimated from ICESat, GPS and GRACE Measurements, *J. Geophys. Res. – Earth*, 122, 76–90, 2017.
- Kendall, R.A., Mitrovica, J.X., and Milne, G.A.: On Post-Glacial Sea Level–II. Numerical Formulation and Comparative Results on Spherically Symmetric Models, *Geophys. J. Int.*, 161, 679–706, 2005.
- 330 Klemann, V., Ivins, E., Martinec, Z., Wolf, D.: Models of active glacial isostasy roofing warm subduction: case of the South Patagonian Ice field. *J. Geophys. Res.* 112, B09405, <http://dx.doi.org/10.1029/2006JB004818>, 2007.
- Kopp, R. E., Horton, R. M., Little, C. M., Mitrovica, J. X., Oppenheimer, M., Rasmussen, D. J., et al.: Probabilistic 21st and 22nd century sea-level projections at a global network of tide gauge sites. *Earth’s Futur.* 2, 383–406, doi:10.1002/2014EF000239, 2014.
- 335 Lambeck, K., Rouby, H., Purcell, A., Sun, Y., and Sambridge, M.: Sea level and global ice volumes from the Last Glacial Maximum to the Holocene. *Proc. Natl. Acad. Sci.*, 201411762, doi:10.1073/pnas.1411762111, 2014.
- Lange, H., Casassa, G., Ivins, E.R., Schröder, L., Fritsche, M., Richter, A., Groh, A., Dietrich, R.: Observed crustal uplift near the Southern Patagonian Icefield constrains improved viscoelastic Earth models. *Geophys. Res. Lett.*, 41, <http://dx.doi.org/10.1002/2013GL058419>, 2014.
- 340 Larour, E., Ivins, E. R., and Adhikari, S.: Should coastal planners have concern over where land ice is melting? *Sci. Adv.* 3, e1700537, 2017.
- Larsen, C.F., Motyka, R.J., Freymueller, J.T., Echelmeyer, K.A., Ivins, E.R.: Rapid viscoelastic uplift in southeast Alaska caused by post-little Ice Age glacial retreat. *Earth Planet. Sci. Lett.*, 237, 548–560, <http://dx.doi.org/10.1016/j.epsl.2005.06.032>, 2005.
- 345 Latychev, K., Mitrovica, J.X., Tromp, J., Tamisiea, M.E., Komatitsch, D. and Christara, C.C.: Glacial Isostatic Adjustment on 3-D Earth Models: A Finite-Volume Formulation, *Geophys. J. Int.*, 161, 421–44, 2005.
- Milne, G.A. and Mitrovica, J.X.: Postglacial Sea-Level Change on a Rotating Earth, *Geophys. J. Int.*, 133, 1–19, 1998.
- Milne, G., Gehrels, W., Hughes, C., and Tamisiea, M.E.: Identifying the causes of sea-level change. *Nat. Geosci.*, 2, 471–478, <https://doi.org/10.1038/ngeo544>, 2009.
- 350 Mitrovica, J.X., Wahr, J., Matsuyama, I., and Paulson, A.: The Rotational Stability of an Ice-Age Earth, *Geophys. J. Int.*, 161, 491–506, 2005.
- Mitrovica, J.X., Gomez, N., Morrow, E., Hay, C., Latychev, K., and Tamisiea, M.E.: On the Robustness of Predictions of Sea Level Fingerprints, *Geophys. J. Int.*, 187, 729–42, 2011.
- Mitrovica, J.X. and Milne, G.A.: On post-glacial sea level, I: General theory, *Geophys. J. Int.*, 154, 253–267, 2003.
- 355 Mitrovica, J.X. and Forte, A.M.: A new inference of mantle viscosity based upon joint inversion of convection and glacial isostatic adjustment data, *Earth Planet. Sci. Lett.*, 225, 177–189, 2004.



- Mitrovica, J.X., Tamisiea, M.E., Davis, J.L., and Milne, G.A.: Polar ice mass variations and the geometry of global sea level change, *Nature*, 409, 1026–1029, 2001.
- Oppenheimer, M., B.C. Glavovic, J. Hinkel, R. van de Wal, A.K. Magnan, A. Abd-Elgawad, R. Cai, M. Cifuentes-Jara, R.M. DeConto, T. Ghosh, J. Hay, F. Isla, B. Marzeion, B. Meyssignac, and Z. Sebesvari, 2019: Sea Level Rise and Implications for Low-Lying Islands, Coasts and Communities. In: IPCC Special Report on the Ocean and Cryosphere in a Changing Climate [H.-O. Pörtner, D.C. Roberts, V. Masson-Delmotte, P. Zhai, M. Tignor, E. Poloczanska, K. Mintenbeck, A. Alegría, M. Nicolai, A. Okem, J. Petzold, B. Rama, N.M. Weyer (eds.)]. In press.
- Peltier, W.R.: The impulse response of a Maxwell Earth, *Rev. Geophys.*, 12, 649–669, 1974.
- 365 Peltier, W.R.: Global Glacial Isostasy and the Surface of the Ice-Age Earth: The ICE-5G (VM2) Model and GRACE, *Ann. Rev. Earth Planet. Sci.*, 32, 111–149, 2004.
- Pfeffer, W., Arendt, A., Bliss, A., Bolch, T., Cogley, J., Gardner, A., . . . Sharp, M.: The Randolph Glacier Inventory: A globally complete inventory of glaciers. *Journal of Glaciology*, 60(221), 537-552, doi:10.3189/2014JG13J176, 2014.
- Pollitz, F.F.: Transient rheology of the upper mantle beneath central Alaska inferred from the crustal velocity field following the 2002 Denali earthquake, *J. Geophys. Res.*, B08407, doi:10.1029/2005JB003672, 2005.
- 370 Richter, A., Ivins, E., Lange, H., Mendoza, L., Schröder, L., Hormaechea, J.L., Casassa, G., Marderwald, E., Fritsche, M., Perdomo, R., Horwath, M. and Deitrich, R.: Crustal Deformation Across the Southern Patagonian Icefield Observed by GNSS, *Earth Planet. Sci. Lett.*, 452, 206–215, 2016.
- Sato, T., Larsen, C.F., Miura, S. Ohta, Y., Fujimoto, H., Sun, W., Motyka, R.J., and Freymuller, J.T.: Re-evaluation of the viscoelastic and elastic responses to the past and present-day ice changes in Southeast Alaska, *Tectonophysics*, 511, 79–88, doi:10.1016/j.tecto.2010.05.009, 2011.
- 375 Shepherd, A., Ivins, E., Rignot, E. et al. Mass balance of the Antarctic Ice Sheet from 1992 to 2017. *Nature* 558, 219–222, <https://doi.org/10.1038/s41586-018-0179-y>, 2018.
- Shepherd, A., Ivins, E., Rignot, E. et al. Mass balance of the Greenland Ice Sheet from 1992 to 2018. *Nature* 579, 233–239, <https://doi.org/10.1038/s41586-019-1855-2>, 2020.
- 380 Slangen, A. B. A., Katsman, C. A., van de Wal, R. S. W., Vermeersen, L. L. A., and Riva, R. E. M.: Towards regional projections of twenty-first century sea-level change based on IPCC SRES scenarios, *Clim. Dyn.*, 38, 1191–1209. doi:10.1007/s00382-011-1057-6, 2012.
- Slangen, A. B. A., Carson, M., Katsman, C. A., van de Wal, R. S. W., Köhl, A., Vermeersen, L. L. A., et al.: Projecting twenty-first century regional sea-level changes, *Clim. Change*, 124, 317–332, doi:10.1007/s10584-014-1080-9, 2014.
- 385 Spada, G.: Glacial Isostatic Adjustment and Contemporary Sea Level Rise: An Overview, *Surv. Geophys.*, 38, 153–185, <https://doi.org/10.1007/s10712-016-9379-x>, 2017.
- van der Wal, W., Barnhoorn, A., Stocchi, P., Gradmann, S., Wu, P., Drury, M., and Vermeersen, B.: Glacial isostatic adjustment model with composite 3-D Earth rheology for Fennoscandia, *Geophys. J. Int.*, 194, 61–77, <https://doi.org/10.1093/gji/ggt099>, 2013.
- 390



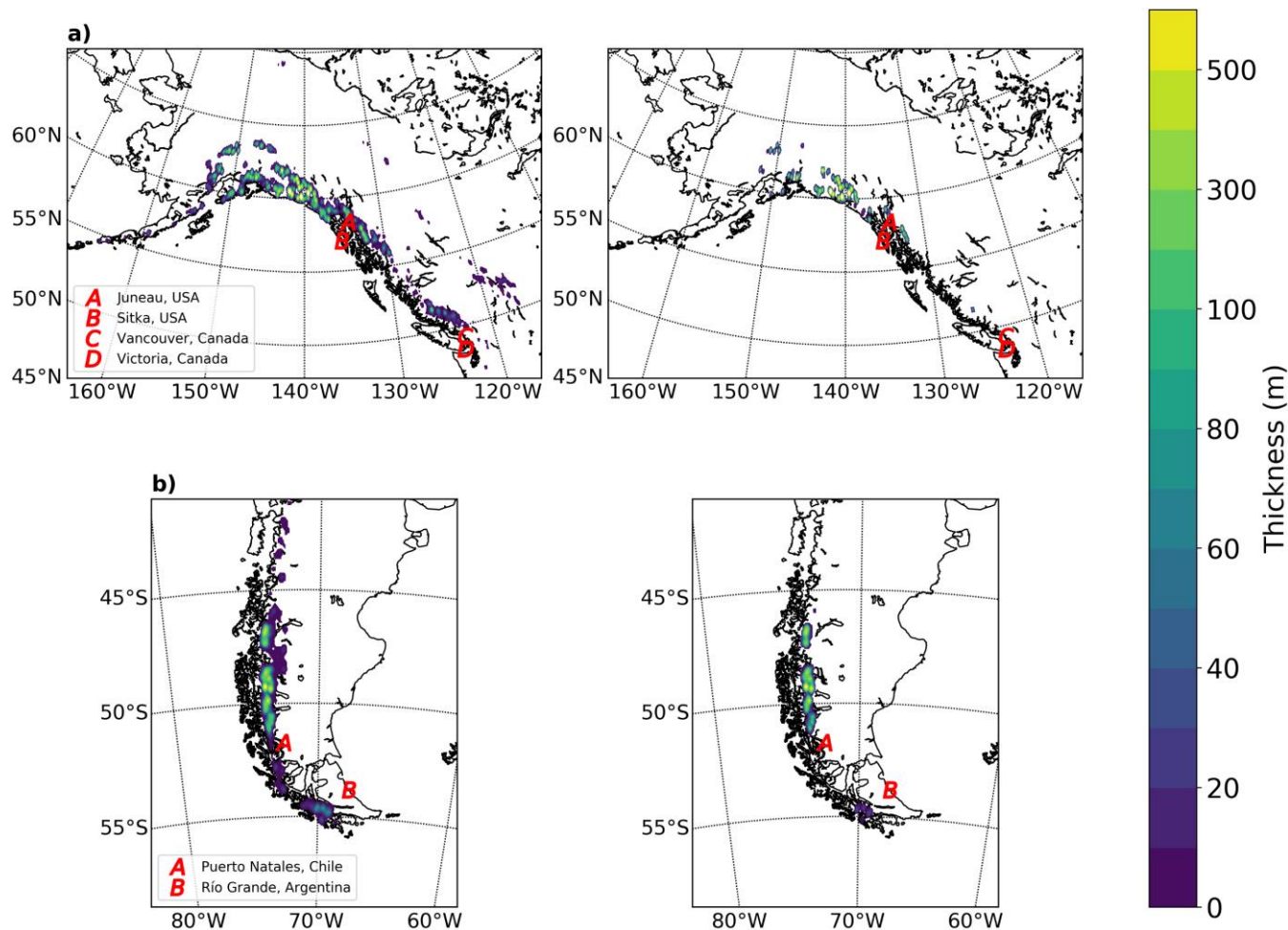
- Vaughan, D.G., J.C. Comiso, I. Allison, J. Carrasco, G. Kaser, R. Kwok, P. Mote, T. Murray, F. Paul, J. Ren, E. Rignot, O. Solomina, K. Steffen and T. Zhang, 2013: Observations: Cryosphere. In: *Climate Change 2013: The Physical Science Basis. Contribution of Working Group I to the Fifth Assessment Report of the Intergovernmental Panel on Climate Change* [Stocker, T.F., D. Qin, G.-K. Plattner, M. Tignor, S.K. Allen, J. Boschung, A. Nauels, Y. Xia, V. Bex and P.M. Midgley (eds.)]. Cambridge University Press, Cambridge, United Kingdom and New York, NY, USA.
- 395
- Whitehouse, P.L.: Glacial isostatic adjustment modelling: historical perspectives, recent advances, and future directions, *Earth Surf. Dynam.*, 6, 401–429, <https://doi.org/10.5194/esurf-6-401-2018>, 2018.
- Whitehouse, P.L., Gomez, N., King, M.A., and Wiens, D.A.: Solid Earth Change and the Evolution of the Antarctic Ice Sheet, *Nat. Comm.*, 10, 1–14, 2019.
- 400
- Wouters, B., Gardner, A. S., and Moholdt, G.: Global Glacier Mass Loss During the GRACE Satellite Mission (2002-2016), *Front. Earth Sci.*, 7, doi:10.3389/feart.2019.00096, 2019.
- Wu, P. and Wang, H.: Postglacial isostatic adjustment in a selfgravitating spherical Earth with power-law rheology, *J. Geodyn.*, 46, 118–130, 2008.
- Yousefi, M., Milne, G.A., Love, R., and Tarasov, L.: Glacial Isostatic Adjustment Along the Pacific Coast of Central North America, *Quat. Sci. Rev.*, 193, 288–311.
- 405
- Yuen, D. A., Sabadini, R. C. A., Gasperini, P., and Boschi, E.: On Transient Rheology and Glacial Isostasy, *J. Geophys. Res.*, 91, 1420–1438, <https://doi.org/10.1029/JB091iB11p11420>, 1986.
- Zemp, M., Huss, M., Thibert, E., Eckert, N., McNabb, R., Huber, J., et al.: Global glacier mass changes and their contributions to sea-level rise from 1961 to 2016, *Nature*, 568, 382–386. doi:10.1038/s41586-019-1071-0, 2019.
- 410
- Zemp, M., Frey, H., Gärtner-Roer, I., Nussbaumer, S.U., Hoelzle, M., Paul, F., Haeberli, W., et al.: Historically Unprecedented Global Glacier Decline in the Early 21st Century, *J. Glaciol.*, 61, 745–762, 2015.

415

420



425



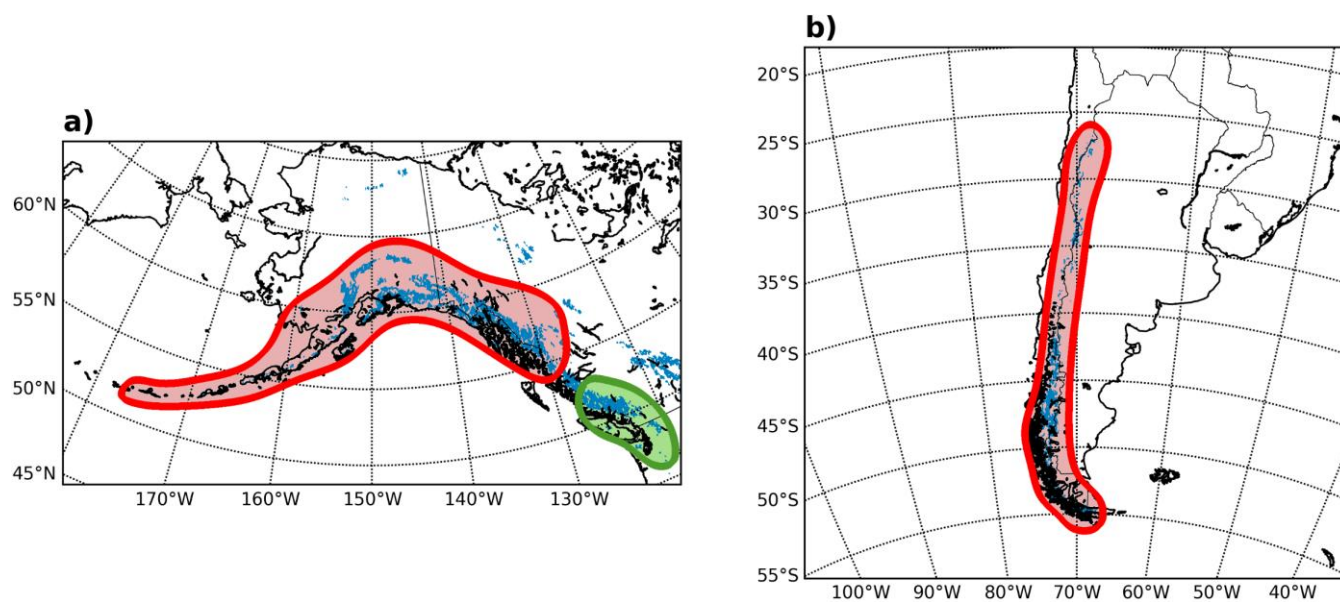
430

**Figure 1.** Estimated spatial distribution in ice thickness in RGI regions 1 & 2 (a) and 17 (b) at the beginning (2010 CE, left) and end (2090 CE, right) of the time period considered. The locations of population centres for which relative sea-level curves are calculated (see Fig. 5) are indicated by the red letters.

435



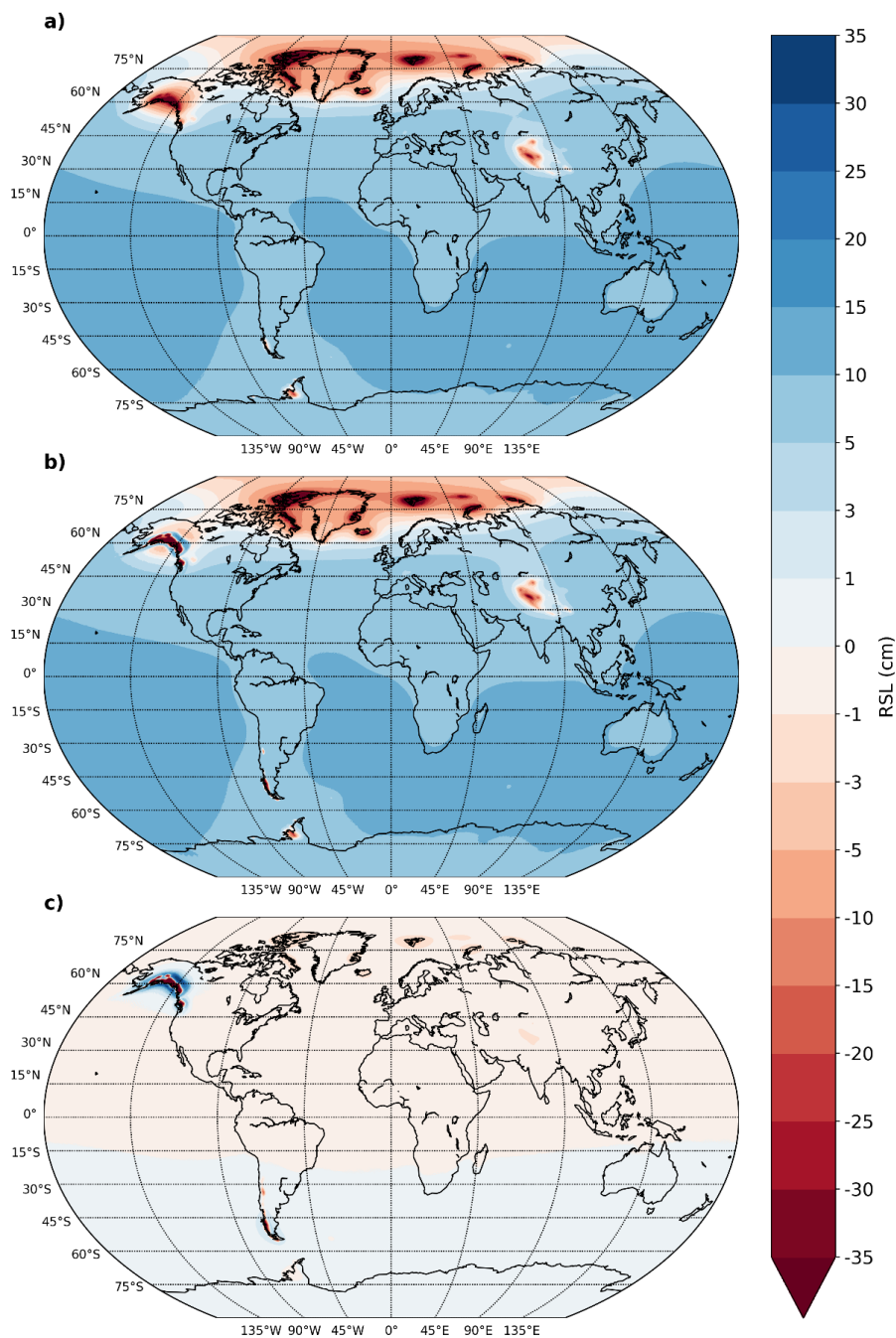
440



445

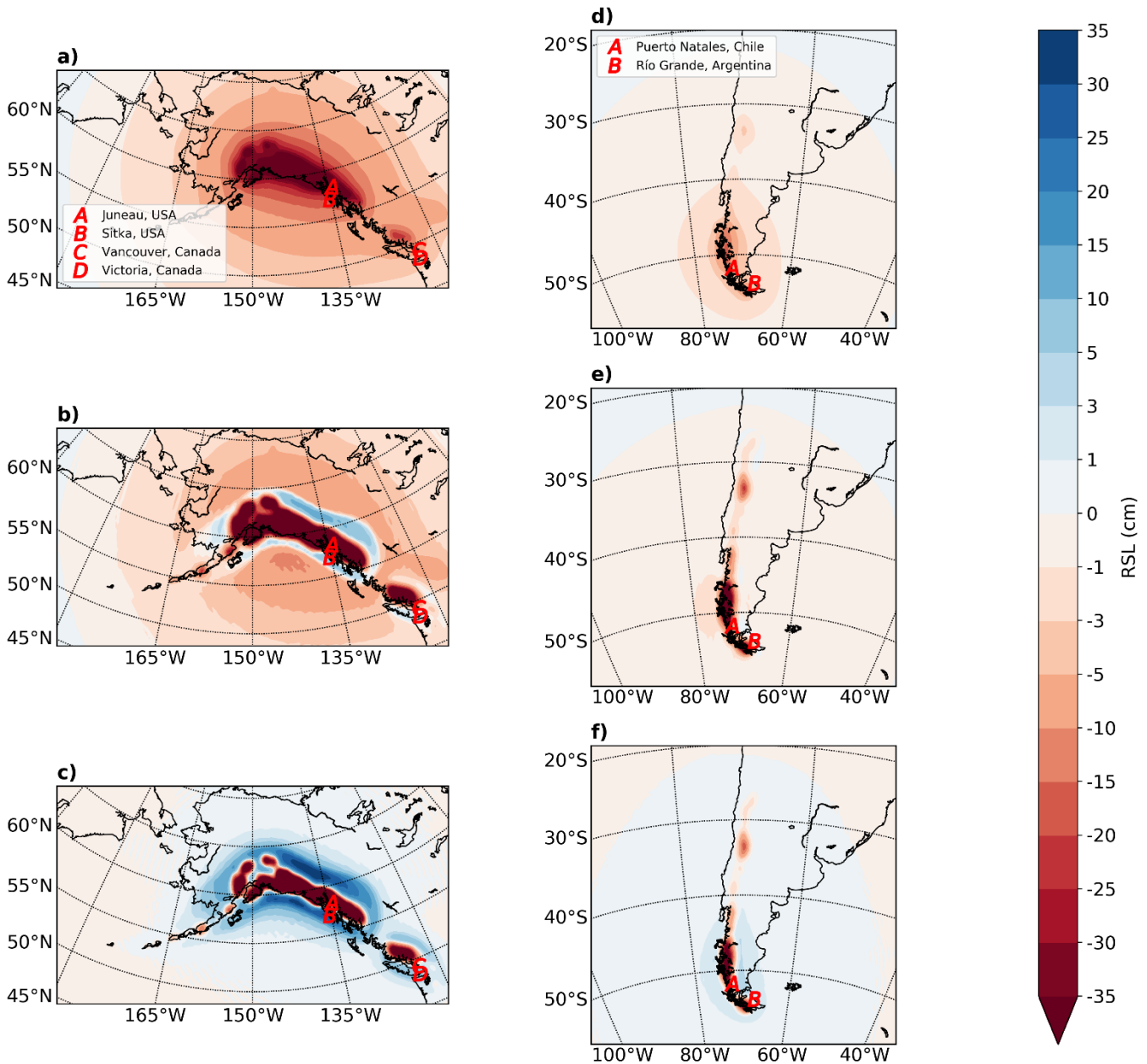
**Figure 2.** Surface lateral extent of the regions for which the underlying Earth structure (lithospheric thickness and sub-lithosphere viscosity profile) deviate from the adopted global values: (a) shows the extent for RGI regions 1 (red) and 2 (green) while frame (b) shows the extent for region 17.

450



455

**Figure 3.** Calculated sea-level fingerprints for estimated changes in global glacier distribution from 2010 to 2100 CE for: (a) a 1-D (spherically symmetric) elastic Earth model and (b) a 3-D viscoelastic Earth model with low viscosity regions located as indicated in Fig. 2. (c) The difference between the viscoelastic and elastic results (i.e. (b) minus (a)).



460

**Figure 4.** Calculated sea-level fingerprints for estimated changes in regional glacier distributions for RGI regions 1 & 2 (left) and region 17 (right). The different frames show results for: (a & c) a 1-D (spherically symmetric) elastic Earth model, (b & d), a 3-D viscoelastic Earth model with low viscosity regions located as indicated in Fig. 2. The results in (c) and (f) show the differences between the elastic and viscoelastic results, respectively (i.e. (b) minus (a) and (d) minus (e)). Note that these results do not include the sea-level signal associated with ice mass changes from outside of the RGI regions shown. The locations of population centres for which relative sea-level curves are calculated (see Fig. 5) are indicated by the red letters.

465



470

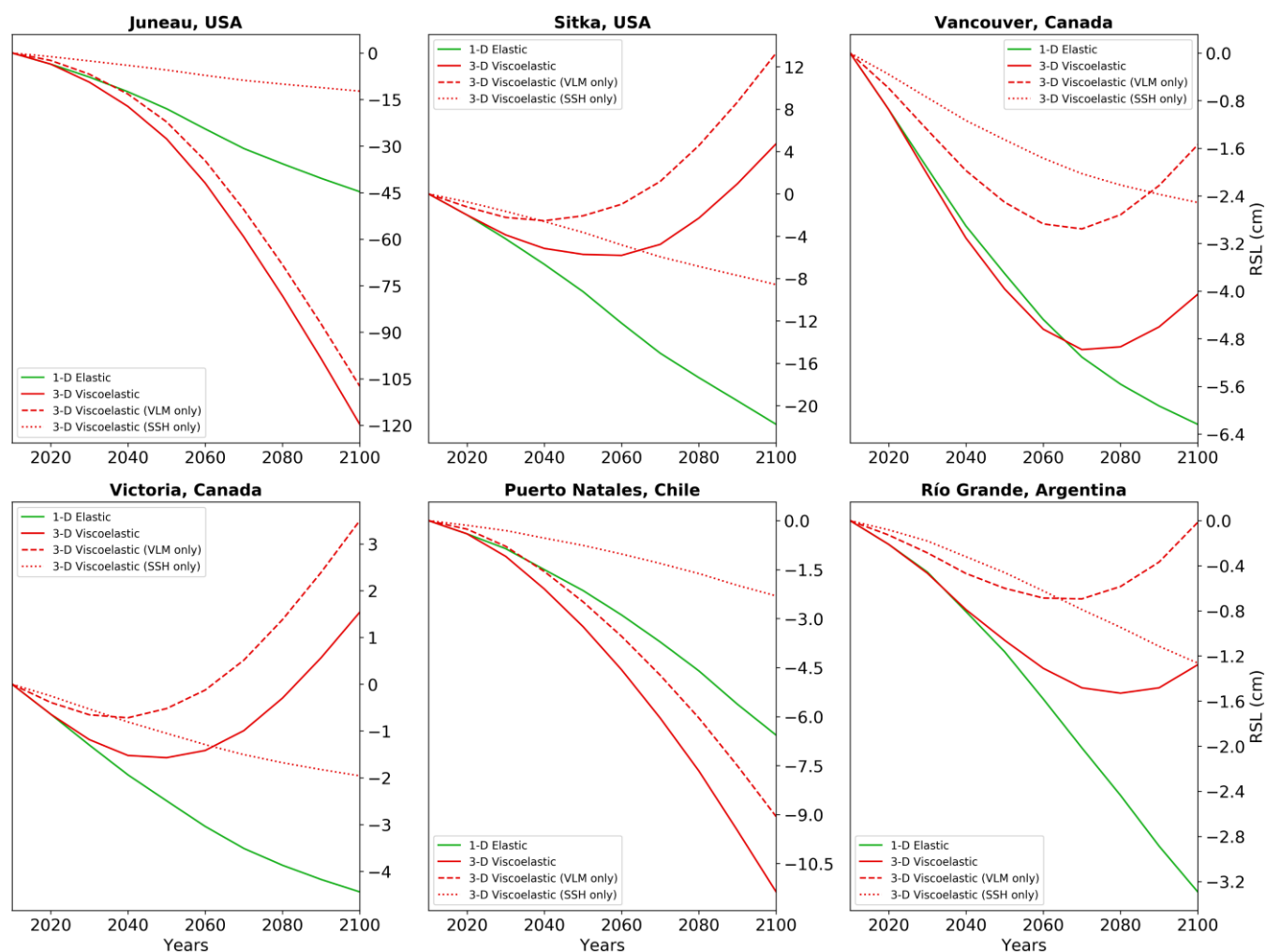


**Figure 5.** Calculated RSL curves showing the time variation of the spatial patterns in Fig. 4 at the locations indicated in Figs 1 and 4. The contributions of vertical land motion (VLM) and sea-surface height (SSH) change to RSL are also shown for the 3-D viscoelastic Earth model. As for Fig. 4, these results do not include the sea-level signal associated with ice mass changes from outside the respective RGI regions.